AUTHOR	Kuusela, Tom A.
TITLE	Methods to depolarize narrow and broad spectrum light
YEAR	2021, September 22th.
DOI	https://doi.org/10.1119/10.0005269
JOURNAL & CITATION	Journal: American Journal of Physics Tom A. Kuusela, "Methods to depolarize narrow and broad spectrum light", American Journal of Physics 89, 963-968 (2021) https://doi.org/10.1119/10.0005269

Methods to depolarize narrow and broad spectrum light

Tom A. Kuusela*

Department of Physics and Astronomy,

University of Turku, 20014 Turku, Finland

(Dated: November 15, 2021)

Abstract

In many optics applications it is important to use well-polarized light. However, there are situations in which randomly polarized light has distinct advantages. We demonstrate two approaches by which a polarized light beam can be totally depolarized, each using a simple setup and inexpensive components. The first method, designed for narrow spectrum light, works by combining the horizontal polarization component of the beam with the delayed vertical component. The second method, which is most suitable for broad spectrum light, uses birefringent quartz plates. In both approaches, the polarization state is characterized by Stokes parameters measured using a rotating quarter-wave plate and fixed polarizer. We measure the coherence function of the electric fields and determine the minimum delay or quartz plate thickness required for decoherence. Coherences are modelled by Gaussian or Lorentzian functions and compared with the spectral properties of the light sources.

I. INTRODUCTION

The polarization state of light is important in many applications. Well controlled linearly or circularly polarized light can be used to probe materials and chemical compounds.[1] However, there are also applications where we require *randomly polarized light*. For example, the efficiency of gratings used in monochromators depends strongly on polarization.[2] In optical single mode fibers, which can maintain polarization for many kilometres, the state of polarization fluctuates randomly due to changes in temperature and external stress. If light is transmitted through a fiber to a polarization-sensitive optical element, significant noise in intensity can be observed.[3] By depolarising the light, these kinds of phenomena can be avoided.

There are many types of depolarizer designs. The oldest one is the Lyot depolarizer.[4] It consists of two wave plates (with thickness ratio 2:1) bonded together and positioned such that their optical axes are oriented 45° apart. The depolarization is based on the group-delay time difference between the polarization modes. Unfortunately, the output is a periodic function of wavelength, so the plate thicknesses must be carefully optimized in each application. The Lyot depolarizer is not practical for depolarising narrow spectrum light because the wave plates must be very thick. Another design is the wedge depolarizer, where two crystal quartz wedges, one of which is twice as thick as the other, are stacked but slightly separated.[5] The output is pseudo-random in polarization: the transmitted beam is not unpolarized, but the polarization varies spatially within the beam.

Quite a different approach is based on the path separation of horizontal and vertical polarization components of the beam. One component is delayed by a long optical fiber and then both components are merged using a beam splitter.[6] This design, used in many commercial depolarizer devices, works well with sources of very narrow bandwidth since a long path difference is easily realized in fibers. The output beam is also truly random in polarization. We use this setup, but without optical fibers, in our first approach. Our second approach is designed for sources of wide spectrum. It uses the birefringence of thick quartz plates to create a compact apparatus with no need for long path differences.[7] The output beam is not pseudo-random, as it is in the case of Lyot or wedge depolarizers, but it is truly randomly polarized.

II. STOKES PARAMETERS

The Stokes parameters are widely used to characterize the polarization state of an optical beam, mainly because they can determined using directly measurable quantities.[8,9] In the case of monochromatic light, these parameters describe the orientation and ellipticity angles of the polarization ellipse. They can also characterize the polarization state of partially and totally unpolarized light.

We choose a Cartesian coordinate system (x, y, z) where x and y are perpendicular to the direction of light propagation z. Then we have (generally complex) orthogonal electric field components $E_x(z,t)$ and $E_y(z,t)$, where t represents time. The Stokes parameters are defined as[10]

$$S_0 = \langle |E_x|^2 \rangle + \langle |E_y|^2 \rangle, \tag{1}$$

$$S_1 = \langle |E_x|^2 \rangle - \langle |E_y|^2 \rangle, \tag{2}$$

$$S_2 = 2\,\mathrm{Re}\langle E_x^* E_y \rangle = \langle E_x^* E_y + E_x E_y^* \rangle, \tag{3}$$

$$S_3 = 2\,\mathrm{Im}\langle E_x^* E_y \rangle = i\langle E_x E_y^* - E_x^* E_y \rangle, \tag{4}$$

where the symbol * indicates the complex conjugate and the brackets $\langle\ \rangle$ time averaging over a long period

$$\langle f(t) \rangle = \lim_{T\to\infty} \int_0^T f(t)dt. \tag{5}$$

The parameter S_0 describes the total intensity, S_1 reflects a tendency for the polarization to be either horizontal or vertical, S_2 a tendency to be diagonal (linearly polarized at 45°) or antidiagonal (linearly polarized at −45°), and S_3 a tendency to right or left circular polarization. The parameters S_2 and S_3 are *coherences* which express how well correlated the electric field components are. When we normalize all Stokes parameters to the total intensity S_0, the first parameter is always equal to 1 and the rest have values in the range $(-1, 1)$. The degree of polarization is

$$DOP = \frac{\sqrt{S_1^2 + S_2^2 + S_3^2}}{S_0}. \tag{6}$$

For completely polarized light $DOP = 1$, but for partially polarized light $0 < DOP < 1$. If light is totally unpolarized, $DOP = 0$, i.e., $S_1 = S_2 = S_3 = 0$.

III. DEPOLARIZING LIGHT

Let us first consider the special case of elliptically polarized monochromatic light of the x and y components

$$E_x(z,t) = E_{0x}\exp[i(kz-\omega t+\delta_x)], \tag{7}$$

$$E_y(z,t) = E_{0y}\exp[i(kz-\omega t+\delta_y)], \tag{8}$$

where E_{0x} and E_{0y} are the field amplitudes, ω is the angular frequency, $k = 2\pi/\lambda$ the wave number, and δ_x and δ_y are constant phases. In order to depolarize the light beam the Stokes parameters S_1, S_2 and S_3 must vanish. The parameter S_1 can be easily set to zero by adjusting the field amplitudes $E_{0x} = E_{0y} \equiv E_0$ by, for example, rotating the polarization plane with a half-wave plate. The remaining parameters are now $S_2 = 2E_0^2\cos(\delta_y - \delta_x)$ and $S_3 = 2E_0^2\sin(\delta_y - \delta_x)$. Clearly, the parameters S_2 and S_3 can never be simultaneously zero. Furthermore, the sum of these coherence terms (normalized by S_0) satisfy the condition $S_2^2 + S_3^2 = 1$.

If the light is not monochromatic but a superposition of many different frequency components $E_{x,l}$ and $E_{y,l}$, which don't necessarily have the same phase difference at all frequencies, we have new possibilities to adjust the coherence related parameters S_2 and S_3. First, assume again that the input beam is divided into horizontal and vertical components with equal amplitudes, i.e., $E_{0x,l} = E_{0y,l} \equiv E_{0,l}$, so $S_1 = 0$. Next set $\delta_{x,l} = \delta_{y,l} \equiv \delta_l$ so that each frequency component is initially diagonally polarized. Finally, introduce the same constant time delay τ in all vertical components by allowing the vertically polarized part of the beam to travel along a longer path than the horizontal component. Then we have new vertical components

$$E'_{y,l}(z,t) = E_{y,l}(z,t+\tau) = E_{0,l}\exp\{i[k_l z-\omega_l(t+\tau)+\delta_l]\} = E_{0,l}\exp\{i[k_l z-\omega_l t+\delta_l-\omega_l\tau]\}, \tag{9}$$

Clearly, each vertical component has an additional phase, the last term in the argument of the exponent function, which depends on the frequency of that component. In practice this means that after recombination the polarization states of all frequency components have a tendency to be different when the time delay increases.

It should be noticed that now the coherence $\langle E_x^*(z,t)E'_y(z,t)\rangle = \langle E_x^*(z,t)E_y(z,t+\tau)\rangle$ has actually the form of the autocorrelation $\langle E^*(z,t)E(z,t+\tau)\rangle$ because in this case the

only difference between horizontal and vertical components is the temporal variable. The autocorrelation is, on the other hand, directly linked to *the degree of the first-order coherence* of light[11]

$$g^{(1)}(\tau) = \frac{\langle E^*(t)E(t+\tau)\rangle}{\langle E^*(t)E(t)\rangle}, \tag{10}$$

when we omit the z coordinate. We can do this since all fields are studied in the same position in space. In general, the coherence varies between 0 and 1. If light is monochromatic, coherence or autocorrelation is always 1, but if there are several frequency components, the coherence can be less than 1 depending on the phase conditions.

When we calculate the coherence $\langle E^*(t)E(t+\tau)\rangle$, where the electric field is a superposition $E(t) = \sum_l E_l \exp(-i\omega_l t)$, the cross-terms ($l \neq m$) are of the form $\langle \exp[i(\omega_l - \omega_m)t] \exp(-i\omega_l \tau)\rangle$, which all vanish (see Appendix). The remaining terms are of the form $\langle \exp(-i\omega_l \tau)\rangle$, which do not vanish but their value depends on the frequency and delay. However, with certain combinations of the amplitudes E_l the autocorrelation approaches zero for *long delays*. In general though, the coherence or autocorrelation is rather difficult to calculate starting directly from the (discrete or continuous) superposition of waves. Instead, we can utilize the *Wiener-Khinchin theorem*, which states that the autocorrelation of the electric field $E(t)$ and the power spectrum of the intensity $S(\omega)$ are a Fourier transform pair[11–13]

$$\langle E^*(t)E(t+\tau)\rangle = \mathscr{F}\{S(\omega)\} = \frac{1}{2\pi}\int_{-\infty}^{\infty} S(\omega)e^{-i\omega\tau}d\omega, \tag{11}$$

$$S(\omega) = \mathscr{F}^{-1}\{\langle E^*(t)E(t+\tau\rangle\} = \int_{-\infty}^{\infty} \langle E^*(t)E(t+\tau\rangle e^{i\omega\tau}d\tau. \tag{12}$$

If we know the power spectrum of the light, we can immediately calculate the autocorrelation of the electric field. In most cases, we can assume that the power spectrum has either *Gaussian* or *Lorentzian* form. The Gaussian spectrum is given by

$$S_G(\omega) = S_0 e^{-\frac{(\omega-\omega_0)^2}{2\sigma^2}}, \tag{13}$$

where S_0 is the scaling factor, ω_0 the central frequency and σ determines the full width at half maximum $FWHM = 2\sigma\sqrt{2\ln(2)}$ of the spectrum. By taking the Fourier transform of this spectrum we get the corresponding first-order coherence

$$g_G^{(1)}(\tau) = e^{-i\omega_0\tau}e^{-\frac{1}{2}(\sigma\tau)^2}. \tag{14}$$

It is obvious that without any time delay we have $|g_G^{(1)}(0)| = 1$ but in the limit $\tau \to \infty$ $|g_G^{(1)}(\tau)| \to 0$, i.e., the autocorrelation of the fields and the Stokes parameters S_2 and S_3 vanish. When we recombine the horizontal and the delayed vertical components into one beam we finally create a totally unpolarized light beam. The calculation proceeds similarly for the Lorentzian, given by

$$S_L(\omega) = S_0 \frac{\gamma/\pi}{\gamma^2 + (\omega - \omega_0)^2}, \tag{15}$$

where 2γ is the $FWHM$ of the spectrum. We obtain

$$g_L^{(1)}(\tau) = e^{-i\omega_0\tau} e^{-\gamma|\tau|}. \tag{16}$$

In this case, too, the autocorrelation vanishes in the limit of long delays.

IV. POLARIZATION STATE ANALYSIS

The classical measurement of the Stokes parameters is carried out by directing the beam through a fixed quarter-wave plate and a rotatable linear polarizer (or rotatable half-wave plate and fixed polarizer) in four different combinations. Here we use another approach in which a rotatable quarter-wave plate is followed by a fixed (transmission axis in the vertical

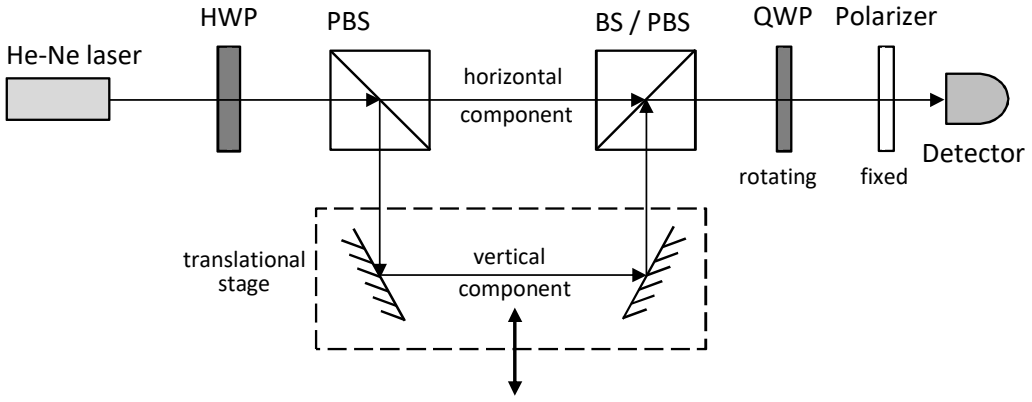

FIG. 1. Experimental setup for a He-Ne laser source. The half-wave plate (HWP) creates diagonal polarization and the polarizing beam splitter (PBS) divides the beam into horizontal and vertical components. The vertical component is delayed and finally both components are merged in the beam splitter (BS). The output beam is analyzed by the rotating quarter-wave plate (QWP) and the fixed polarizer.

direction) linear polarizer (see Fig.1).[14,15] The intensity of the optical beam, after passing through the quarter-wave plate and polarizer, is a function of the rotation angle θ (the fast axis angle measured from the vertical):

$$I(\theta) = \frac{1}{2}\left[A + B\sin(2\theta) + C\cos(4\theta) + D\sin(4\theta)\right]. \tag{17}$$

The coefficients A, B, C and D are related to the Stokes parameters as follows:

$$S_0 = A - C,\ S_1 = 2C,\ S_2 = 2D,\ S_3 = B. \tag{18}$$

The coefficients in Eq. (17) can be determined using Fourier analysis but we fit the intensity function $I(\theta)$ directly to the measured values for θ in the range 0 to 180° in steps of 10°. This method has several advantages over the classical one. In the classical method the transmission axis of the polarizer must be carefully aligned to the required angles (0°, 45° and 90°); the absorption of the quarter wave plate easily introduces errors; and because there are only 4 measurements, it is more difficult to achieve good accuracy. By using a rotating quarter-wave plate, these difficulties can be mostly avoided.

V. EXPERIMENTS

A. Narrow-band source: a He-Ne laser

In our first experiment, we measured the autocorrelation of a He-Ne laser as a function of the delay τ. The laser (Uniphase 1507P) has an output power of 0.5 mW and a polarization ratio 500:1. A half-wave plate is used to balance the horizontal and vertical intensities in order to fulfill the condition $S_2 = 0$. The vertical component of the light beam is delayed by two mirrors which are assembled on a movable plate (see Fig. 1). The plate is slid over the surface of the optical table while abutting a long guiding slab oriented parallel to the direction of travel. This allows us to change the delay without changing the direction of the beam (if a long optical rail is available, it could also be used). We can adjust the path difference in the range of 20 to 1000 mm corresponding to a delay of 0.13 to 3.33 ns.

The apparatus shown in Fig. 1 must be aligned so that both beams overlap as much as possible after the second beam splitter. Interferometric accuracy in the alignment is not needed, as long as both beams hit the surface of the detector. Any intensity detector can be used but it must be linear. A detector of large active area facilitates adjustments;

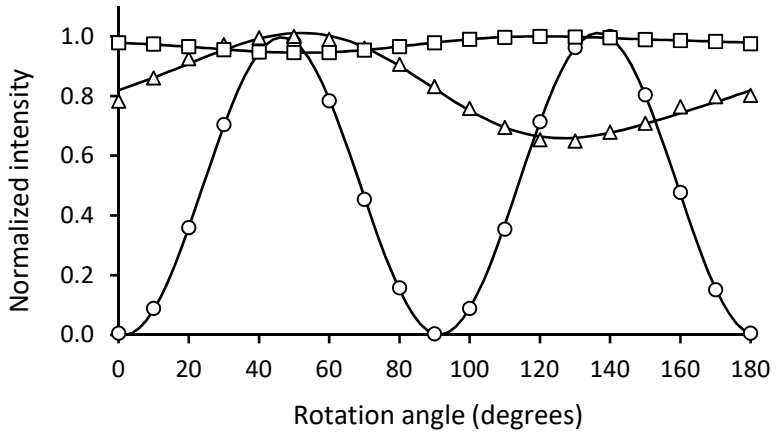

FIG. 2. He-Ne laser source: intensity as a function of the rotation angle of the quarter-wave plate with path differences of 0 mm (circles), 70 mm (triangles) and 300 mm (squares). The lines are fits to Eq. (17).

our detector (Thorlabs photodiode S120VC) has a diameter of 9 mm. The polarization is measured using the method described above. The intensity as a function of the rotation angle of the quarter wave plate is shown in Fig. 2 for several path differences. For clarity, all intensities are scaled to have the maximum value of 1. The case of zero path difference is measured by blocking the vertical component. Clearly, intensity modulation decreases as the path difference increases and the light beam becomes more depolarized.

The first-order coherence as a function of the delay is presented in Fig. 3. At zero delay, we use the degree of polarization instead of the coherence since we have only the horizontal component, as mentioned above. The measured values are best fitted by the Lorentzian coherence of Eq. (16) with $\gamma = 1.019$ GHz ($\omega_0 = 4.74$ THz corresponding to the wavelength of 632.2 nm)[16]. This corresponds to a full width at half maximum value $FWHM = 2.04$ GHz. We did not measure the actual power spectrum of the He-Ne laser output because it is a rather challenging task and requires expensive equipment that is typically not available in student labs.

The spectral distribution of He-Ne laser light is governed both by the atomic (fluorescence) line shape of the active medium and by the longitudinal cavity modes.[13,17]Inhomogeneous Doppler broadening, arising from the random thermal motion of neon atoms, yields a Gaussian line shape with $FWHM$ of about 2 GHz, the same magnitude as we found but with a different line shape. However, in practice the situation is more complex, due to mode

competition and other mechanisms. Using the Gaussian model (Egn. 14) to fit our data, we get almost the same result $FWHM = 2.00$ GHz. Finally, from Fig. 3 we can see that a time delay of about 1 ns is needed to have very low coherence ($DOP = 0.029$), i.e., the path length difference should be more than 30 cm for creating unpolarized light.

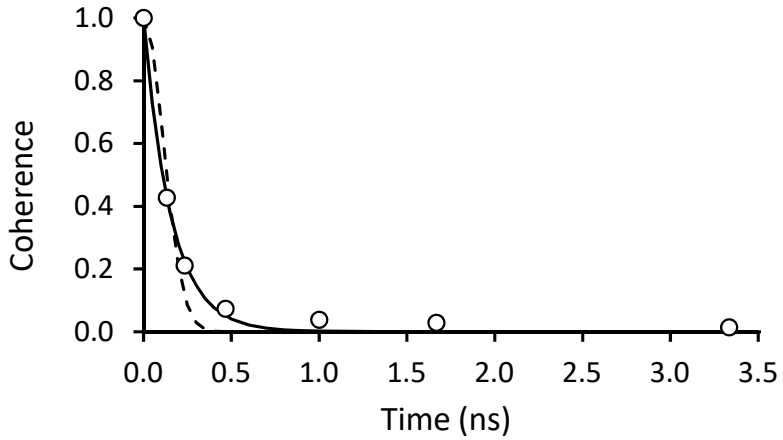

FIG. 3. He-Ne laser source: First-order coherence as a function of the time delay (circles), and numerically fitted Lorentzian (thin line) and Gaussian (dashed line) model.

The measured coherence, especially when it is close to zero, is sensitive to the balance between horizontal and vertical polarization components, which should be always checked when the path length is changed. An additional source of error is that most polarizing beam splitters create a highly polarized transmitted beam, but the reflected beam is less highly polarized, with an extinction ratio as low as 20:1. If necessary, an additional polarizer can be added to the path of the vertical component in order to eliminate any horizontal component from the delayed portion of the beam.

B. Broad-band source: a light emitting diode

When the spectral distribution is very narrow, the delay between the horizontal and vertical polarization components can be created as in the previous case of He-Ne laser source. If the spectral distribution is wide, the necessary minimum path difference is very short and the setup described in Fig. 1 can be somewhat cumbersome. As an example we use a light emitting diode (LED) followed by an interference band-pass filter and a polarizer (see Fig. 4). Instead of using a physical path length difference between the horizontal and vertical

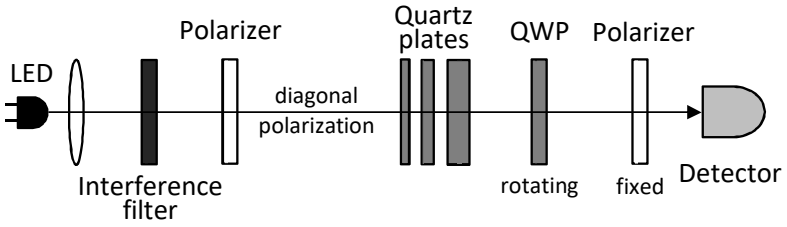

FIG. 4. Experimental setup for a LED source. Light from the light emitting diode (LED) is collimated by a lens and passed through a narrow band interference filter. The polarizer creates diagonal polarization. The horizontal and vertical components of the beam undergo different delay times in the set of birefringent quartz plates. The output polarization is analyzed as in the previous case.

components of the beam, we guide the beam through a set of quartz plates. Quartz is a birefringent material with two refractive indexes, the ordinary (fast) n_o and extraordinary (slow) n_e, and $n_o < n_e$. When a linearly polarized light beam passes through a quartz plate whose fast (or slow) axis is at a 45° angle relative to the direction of the polarization, the time delay between the horizontal and vertical components after the plate is

$$\Delta t = \Delta t_e - \Delta t_o = \frac{l}{c/n_e} - \frac{l}{c/n_o} = \frac{0.0091}{c} l, \tag{19}$$

where l is the thickness of the plate, c the velocity of light, and the refractive indexes are $n_o = 1.5425$ and $n_e = 1.5516$ at a wavelength of 635 nm.[18] We use a red LED and an interference filter with the central wavelength 635 nm and bandwidth 10 nm (Thorlabs FL635-10), so that we can use the same quarter-wave plate as in the previous example to analyze polarization (see Fig. 4). Our set of quartz plates has thicknesses of 2, 5 and 10 mm (Newlight Photonics QAR25 200/500-A and QAT12100-A) and we use them in various combinations to obtain time delays up to 0.5 ps. If multi-order wave plates are available, they can also be used.

The intensity as a function of the rotation angle of the quarter wave plate is shown in Fig. 5 with several quartz plate thicknesses. As expected, the intensity modulation decreases with increasing plate thickness. The first-order coherence (Eq. 10) as a function of the time delay is displayed in Fig. 6. In this case, Gaussian type coherence of Eq. (14) describes the experimental results reasonably well with $\sigma = 2.322$ THz, or $FWHM = 5.47$ THz. Since the spectrum of this source is rather wide, the quarter-wave plate is not ideal and this produces some inaccuracy in polarization state analysis. For example, DOP is clearly less

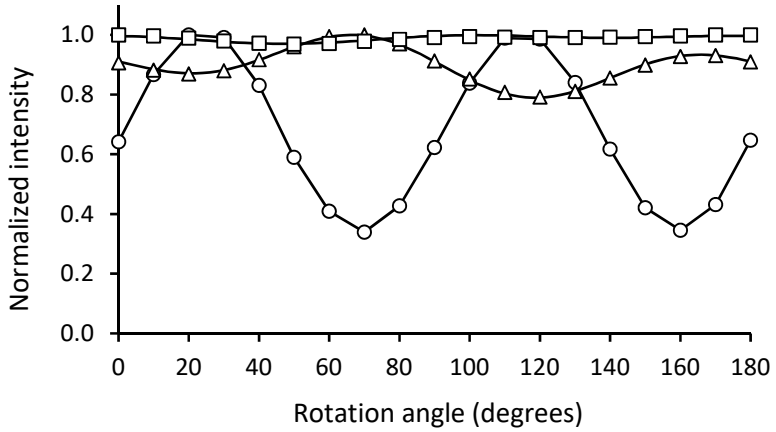

FIG. 5. LED source: intensity as a function of the rotation angle of the quarter-wave plate with the total quartz plate thickness of 0 mm (circles), 5 mm (triangles) and 12 mm (squares). The lines are fits to Eq. (17).

than 1 when there are no quartz plates (the data point corresponding to zero time in Fig. 6).

We also measure the spectrum of the LED output before and after the interference filter (Thorlabs Spectrometer CCS100) (see Fig. 7). The filtered output is not exactly Gaussian but the numerical fit of the spectrum (Eq. 13) gives $\sigma = 2.328$ THz, very close to the value found in the coherence analysis. Based on the measurements shown in Fig. 6, we can conclude that the light beam is highly depolarized ($DOP = 0.019$) when the total thickness of the quartz plates is about 12 mm.

C. Concluding remarks

The experimental setup in Fig. 4 not only has pedagogical interest but it is also an essential part of some novel approaches used in quantum optics. In studies of *open quantum systems* we are interested in effects due to the interaction of the environment on quantum systems, in order to find ways to decrease or even eliminate such effects when looking for practical implementations of quantum computing and secure data protocols. In laboratory experiments used to explore these phenomena, however, it is rather difficult to control interactions between a quantum system and its environment, and so more feasible models or simulations are needed. In the simplest quantum system, we use the polarization degree of freedom (DOF) of single photons as a model of a qubit, and normally ignore the frequency

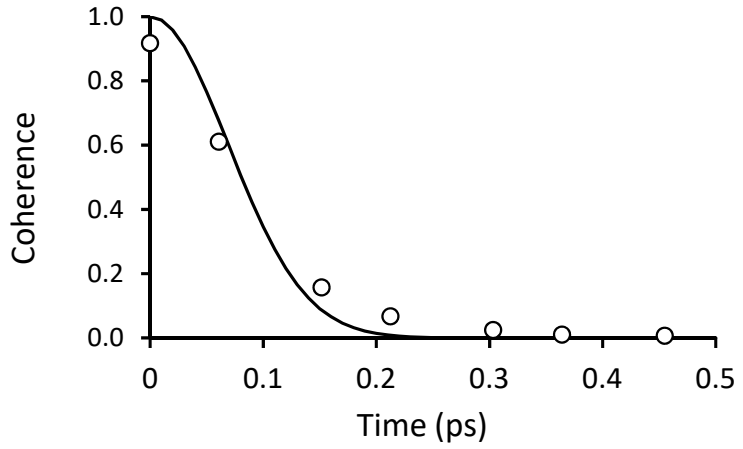

FIG. 6. LED source: First-order coherence as a function of the time delay (circles) and numerically fitted Gaussian model (thin line). The experimental data points correspond to the quartz plate thicknesses of 0, 2, 5, 7, 10, 12 and 15 mm.

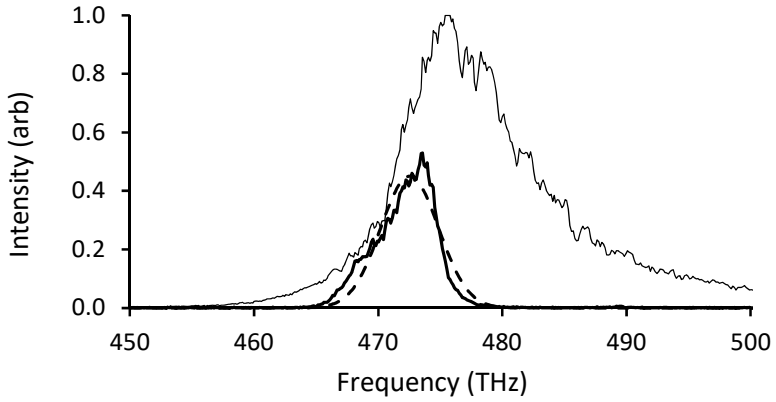

FIG. 7. Spectrum of the LED source before (thin line) and after the interference filter (thick line), and the fitted Gaussian profile (dashed line).

DOF because we are not interested in it. However, this latter *DOF* (the spectral property of the photons), which can be rather easily controlled in practical single photon sources, can play the role of the environment. In a birefringent quartz plate this "co-moving" (in the sense that it travels with photons) environment is coupled to the polarization, i.e., the horizontal and vertical polarization components of the photon experience different phase shifts. The thickness of the plate determines the interaction time between the photon and the environment.[7,19]. As a result, the originally pure polarization state of the photon qubit experiences decoherence and the quantum state is not pure but more or less mixed, just as the degree of polarization decreases in the classical picture of light. In more complex

quantum systems, as two entangled photon qubits, the dynamics of decoherence is more complicated and it has no more classical counterpart.

Appendix A: Wiener-Khinchin theorem

Let us assume that the electric field is given (we omit the z-coordinate) by the superposition

$$E(t) = \sum_l E_l e^{-i\omega_i t}. \tag{A1}$$

When we calculate the autocorrelation function $\langle E^*(t)E(t+\tau)\rangle$, we obtain terms

$$\frac{1}{T}\int_0^T E_l e^{i\omega_l t} E_m e^{-i\omega_m(t+\tau)} dt = E_l E_m e^{-i\omega_m \tau}\frac{1}{T}\int_0^T e^{i(\omega_l-\omega_m)t} dt. \tag{A2}$$

In the case of different frequencies ($l \neq m$) we can use the Euler's formula $e^{ix} = \cos(x) + i\sin(x)$ in the integral. Then we have the real part

$$E_l E_m e^{-i\omega_m\tau}\frac{1}{T}\int_0^T \cos[(\omega_l-\omega_m)t]dt = E_l E_m e^{-i\omega_m\tau}\frac{1}{T}\frac{\sin[(\omega_l-\omega_m)T]}{\omega_l-\omega_m}. \tag{A3}$$

Since the value of sin function is restricted, these terms vanish in the limit $T \to \infty$. The imaginary part is

$$E_l E_m e^{-i\omega_m\tau}\frac{1}{T}\int_0^T \sin[(\omega_l-\omega_m)t]dt = E_l E_m e^{-i\omega_m\tau}\frac{-1}{T}\left\{\frac{\cos[(\omega_l-\omega_m)T]}{\omega_l-\omega_m} - \frac{1}{\omega_l-\omega_m}\right\}. \tag{A4}$$

The value inside the braces is restricted, and so these terms also vanish in the limit $T \to \infty$. With equal frequencies ($l = m$), Eq. (A2) has the form

$$E_l^2 e^{-i\omega_l\tau}\frac{1}{T}\int_0^T dt = E_l^2 e^{-i\omega_l\tau}, \tag{A5}$$

which does not vanish. The intensity of the component at the frequency ω_l is $I_l = E_l^2$. If there are very many frequency components in the superposition of Eq. (A1), the summation can be replaced by integration over the frequency ω, and $I_l \to \frac{1}{2\pi}S(\omega)d\omega$ where $S(\omega)$ is the spectral density. Finally we can write

$$\langle E^*(t)E(t+\tau)\rangle = \frac{1}{2\pi}\int_{-\infty}^{\infty} S(\omega)e^{-i\omega\tau}d\omega. \tag{A6}$$

The right hand side of Eq. (A6) is the Fourier transform $\mathscr{F}\{S(\omega)\}$ of the spectral density.

---

* tom.kuusela@utu.fi

[1] M. Bass, *Handbook of Optics: Volume I, Third Edition* (McGraw-Hill Professional, New York, 2010).

[2] E. G. Loewen, M. Neviere, and D. Maystre,"Grating efficiency theory as it applies to blazed and holographic gratings," Appl. Opt. **16**, 2711–2721 (1977).

[3] B. Hillerich and E. Weidel,"Polarization noise in single mode fibers and its reduction by depolarizers," Opt. Quantum Electron **15**, 281–287 (1983).

[4] B. H. Billings,"A monochromatic depolarizer," J. Opt. Soc. Am. **41**, 966–975 (1951).

[5] J. C. G. de Sande, M. Santasiero, G. Piquero, and F. Gori,"Longitudinal polarization periodicity of unpolarized light passing through a double wedge depolarizer,"Opt. Express **20**, 27348–27360 (2012).

[6] K. Takada, K. Okamoto, and J. Noda,"New fiber-optic depolarizer," J. Lightwave Techn. **4**, 213–219 (1986).

[7] P. G. Kwiat, A. J. Berglund, J. B. Altepeter, and A. G. White,"Experimental verification of decoherence-free subspaces," Science **290**, 498–501 (2000).

[8] E. Hecht,"Note on an operational definition of the Stokes parameters," Am. J. Phys. **38**, 1156–1158 (1970).

[9] E. Collet,"The description of polarization in classical physics," Am. J. Phys. **36**, 713–725 (1968).

[10] H. G. Berry, G. Gabrielse, and A. E. Livinston,"Measurement of the Stokes parameters of light," Appl. Opt. **16**, 3200–3205 (1977).

[11] R. Loudon, *The Quantum Theory of Light* (Oxford University Press, New York, 2000).

[12] C. Chatfield, *The Analysis of Time Series – An Introduction* (Chapman and Hall, London, 1989).

[13] I. R. Kenyon, *The Light Fantastic: A Modern Introduction to Classical and Quantum Optics* (Oxford University Press, New York, 2011).

[14] B. Schaefer, E. Collet, R. Smyth, D. Barret, and B. Fraher,"Measuring the Stokes polarization parameters," Am. J. Phys. **75**, 163–168 (2007).

[15] S. Bobach, A. Hidic, J. J. Arlt, and A. J. Hilliard,"Note: A portable rotating waveplate polarimeter," Rev. Sci. Instrum. **88**, 036101-1–3 (2017).

[16] We use here the unit Hz, not the original unit rad/s of the angular velocity. This simplifies comparisons with literature values and data from the spectrometer.

[17] B. E. A. Saleh and M. C. Teich, *Fundamentals of Photonics 2nd Edition* (Wiley, New Jersey, 2007)

[18] G. Ghosh,"Dispersion-equation coefficients for the refractive index and birefringence of calcite and quartz crystals," Opt. Commun. **163**, 95-102 (1999). See also https://refractiveindex.info

[19] B-H. Liu, L. Li, Y-F. Huang, C-F. Li, G-C. Guo, E-M. Laine, H-P Breuer, and J. Piilo,"Experimental control of the transition from Markovian to non-Markovian dynamics of open quantum systems," Nat. Phys. **7**, 931–934 (2011).